# A survey of diamagnetic probes for copper$^{2+}$ binding to the prion protein. $^{1}$H NMR solution structure of the palladium$^{2+}$ bound single octarepeat†

**Anthony P. Garnett, Christopher E. Jones and John H. Viles***

***Received 15th August 2005, Accepted 27th September 2005***
***First published as an Advance Article on the web 27th October 2005***
**DOI: 10.1039/b511553a**



The prion protein ($PrP^{C}$) is a copper binding cell surface glycoprotein which when misfolded causes transmissible spongiform encephalopathies. The cooperative binding of $Cu^{2+}$ to an unstructured octarepeat sequence within $PrP^{C}$ causes profound folding of this region. The use of NMR to determine the solution structure of the octarepeat region of PrP with $Cu^{2+}$ bound has been hampered by the paramagnetic nature of the $Cu^{2+}$ ions. Using NMR we have investigated the binding of candidate diamagnetic replacement ions, to the octarepeat region of PrP. We show that $Pd^{2+}$ forms diamagnetic complexes with the peptides HGGG, HGGGW and QPHGGGWGQ with 1 : 1 stoichiometry. The $^{1}$H NMR spectra indicate that these peptides are in slow-exchange between free and bound $Pd^{2+}$ on the chemical-shift time-scale. We demonstrate that the Pd–peptide complex forms slowly with a time taken to reach half-maximal signal of 3 hours. Other candidate metal ions, $Ni^{2+}$, $Pt^{2+}$ and $Au^{3+}$, were investigated but only the $Pd^{2+}$ complexes gave resolvable $^{1}$H NMR spectra. We have determined the solution structure of the QPHGGGWGQ–Pd 1 : 1 complex using 71 NOE distance restraints. A backbone RMSD of 0.30 Å was observed over residues 3 to 7 in the final ensemble. The co-ordinating ligands consist of the histidine imidazole side chain Nε, the amide N of the second and third glycines with possibly $H_2O$ as the fourth ligand. The co-ordination geometry differs markedly from that of the HGGGW–Cu crystal structure. This survey of potential replacement metal ions to $Cu^{2+}$ provides insight into the metal specificity and co-ordination chemistry of the metal bound octarepeats.

## Introduction

The prion protein $PrP^{C}$ is a cell surface glyco-protein that is highly conserved across several phyla and widely expressed in several cell types, particularly neurons of the central nervous system where it is GPI anchored largely on the pre-synaptic membrane.[1–3] The misfolding of cellular prion protein is associated with fatal neurodegenerative diseases that are collectively described as spongiform encephalopathies. Prion diseases include Creutzfeldt–Jacob disease (CJD) in humans, bovine spongiform encephalopathy (BSE) in cattle and scrapie in sheep. The infectious agent, which is devoid of nucleic acid, is a proteinous infectious particle, or 'prion'.[4] Prion diseases are characterized by the accumulation of an abnormally folded isoform of the cellular prion protein ($PrP^{C}$) into the misfolded scrapie isoform ($PrP^{Sc}$), which is rich in β-sheets.[1–3]

$PrP^{C}$ contains two distinct structural domains.[5–8] The N-terminal region, residues 23–126, has little defined structure in the absence of $Cu^{2+}$ ions[7] and has a high degree of main-chain flexibility[9] although some ordering is observed at low pH.[10] In contrast, the C-terminal domain, residues 121–231, is largely α-helical.[5] The unstructured N-terminal domain contains an octapeptide sequence, PHGGGWGQ, which is repeated four times between residues 60–91. This octarepeat region binds four $Cu^{2+}$ ions cooperatively.[11–14] In addition we have recently shown that two $Cu^{2+}$ ions bind to a region, outside of the octarepeats, between residues 90 and 126 where $Cu^{2+}$ binding is centered at His111 and His96 and promotes the formation of β-sheet in a region of PrP vital for prion propagation.[15,16]

The normal physiological function of the prion protein is yet to be established but the ability of $PrP^{C}$ to bind $Cu^{2+}$ *in vivo* and *in vitro* suggests a role in copper homeostasis.[17,11] $PrP^{C}$ undergoes constitutive endocytosis that is dependent on the N-terminal domain (residues 23–107), and $Cu^{2+}$ has been suggested to be either required for, or alter the rate of, internalization of PrP.[18,19] Interestingly, a mutant form of PrP associated with familial prion disease contains nine additional octarepeats and fails to undergo copper mediated endocytosis.[19] In contrast recent studies have shown that even in the absence of copper, mouse $PrP^{C}$ is still rapidly endocytosed.[20] Furthermore, PrP expression levels do not seem to affect copper delivery.[21,22] $PrP^{C}$ expression increases the binding of copper to the outer plasma cell membrane and increases antioxidant enzyme activities.[21] It is also suggested that $PrP^{C}$ plays a protective role by binding $Cu^{2+}$ in a redox inactive state.[23,24] An enzymatic role for Cu–PrP has also been proposed as it exhibits superoxide dismutase activity.[25–28]

In prion disease metal binding to the prion protein is altered[29] and metal imbalances are a feature of prion disease.[30] $PrP^{Sc}$ isolated

*School of Biological Sciences, Queen Mary, University of London, Mile End Road, London, UK E1 4NS. E-mail: j.viles@qmul.ac.uk; Fax: +44 (0)20 8983 0973; Tel: +44 (0)20 7882 3054*

† Abbreviations used: PrP, prion protein; $PrP^{Sc}$, scrapie isoform of PrP; $PrP^{C}$, cellular isoform of PrP; CJD, Creutzfeldt–Jacob disease; GPI, glycosyl-phosphatidylinositol; BSE, bovine spongiform encephalopathy; CD, circular dichroism; EPR, electron paramagnetic resonance; NMR, nuclear magnetic resonance; ROESY, rotating frame Overhauser exchange spectroscopy; TOCSY, total correlation spectroscopy; NOESY, nuclear Overhauser exchange spectroscopy.

from diseased brain is found to be metal occupied[31] and copper content at a cellular level is modulated by scrapie infection.[32] In addition, $Cu^{2+}$ can convert the cellular prion protein into a protease-resistant species.[33] Different protease profiles of PrP, observed with and without the presence of $Cu^{2+}$ ions, correspond to similar profiles seen in different strains of prion disease.[34,31] Copper induced redox damage of PrP is implicated in prion disease.[35,36] In addition, disease progression in infected mice has been reported to slow with the use of copper specific chelation therapy.[37] The role of copper in prion diseases, as well as in the normal function of PrP, has been the subject of a number of reviews.[38–43]

The precise structure of the N-terminal octameric repeat region with bound copper has yet to be fully established. However, it is clear that binding of copper causes the region to undergo a profound conformational change to a more ordered state.[11,12] A crystal structure of the copper bound HGGGW motif has been reported[14] which shows $Cu^{2+}$ co-ordinated with 3N and 1O equatorial ligands and an axial water molecule to form a square-pyramidal geometry. The crystal structure is consistent with the EPR data suggesting type II co-ordination geometry.[11,13] The EPR spectra of Cu–HGGGW are indistinguishable from larger multiple repeats[11,13] and so represent the co-ordination of $Cu^{2+}$ to a full single octarepeat. However, the crystal structure of HGGGW does not explain the co-operative nature of copper binding found in multiple repeats. Evidence from circular dichroism indicates that the four octarepeats do not form isolated $Cu^{2+}$ binding motifs, but rather fold up co-operatively within multiple repeats,[12] but the mechanism for this co-operative binding is still unclear.

To date, crystallisation of $Cu^{2+}$ bound multiple repeats has been unsuccessful. Paramagnetic broadening of specific $^1$H NMR signals indicates histidine co-ordination but the paramagnetic $Cu^{2+}$ ion makes structure determination by NMR difficult.[11] However, a diamagnetic replacement ion for $Cu^{2+}$ would facilitate the use of NMR in structure determination. For this reason we have used NMR and optical spectroscopy to investigate the binding of other diamagnetic metal ions to the octarepeat region of PrP. Early work on metal binding to PrP suggests that PrP is quite specific for $Cu^{2+}$ ions.[44] However, $Ni^{2+}$ ions are known to form low-spin diamagnetic square-planar complexes and to mimic type II $Cu^{2+}$ binding.[45,46] The metal ions; $Pd^{2+}$, $Pt^{2+}$ [47] and $Au^{3+}$,[48,49] are also good candidates as diamagnetic probes of $Cu^{2+}$ binding. $Au^{3+}$ is known to form imidazole–$Au^{3+}$ bridged complexes at pH 6–7[48] and thus $Au^{3+}$ is also a candidate as a probe to investigate histidine bridging in PrP metal co-ordination, as has been suggested to occur in the PrP octarepeat–Cu complex,[11] although studies using EPR appear to rule out a bridged species.

We have used HGGG, HGGGW, QPHGGGWGQ, PrP(2octa) and PrP(4octa) peptides as models of the N-terminus octarepeat metal binding domain of PrP. $^1$H NMR and optical spectroscopy have been used to assess $Ni^{2+}$, $Pd^{2+}$, $Pt^{2+}$ and $Au^{3+}$ ions for their suitability as a diamagnetic probe of $Cu^{2+}$ binding. In particular we have characterised the binding of $Pd^{2+}$ to HGGG, HGGGW and QPHGGGWGQ by $^1$H and $^{13}$C NMR spectroscopy. Understanding the structure of the $Cu^{2+}$ bound octarepeats should give us insight into the reasons for PrP's specificity, affinity and folding associated with $Cu^{2+}$ binding.

## Experimental

### Peptide synthesis and purification

Peptides representing various lengths of the repeat region of PrP were synthesised employing solid phase F-moc (*N*-(9-fluorenyl)methoxycarbonyl) chemistry (A.B.C. Imperial College London.) After removing from the resin and de-protection the samples were purified using reverse-phase HPLC and characterised using mass spectrometry and $^1$H NMR. In order to mimic the peptides within the full-length prion protein all peptides were blocked at the N-terminus with *N*-acetyl and at the C-terminus with ethyl ester. Peptides synthesised included the following from the human (PrP) sequence: HGGG; HGGGW; PrP(1octa) QPHGGGWGQ; PrP(2octa, 73–91) WGQPHGGG-WGQPHGGGWGQ; PrP(4octa, 58–91) QPHGGGWGQPHG-GGWGQPHGGGWGQPHGGGWGQ.

### Titration of metal ions

Peptide solution concentrations were measured using the extinction coefficient of tryptophan at 280 nm using the formula: $n \times 5690$ $M^{-1}cm^{-1}$ where $n$ = the number of tryptophan residues present.[50] Typically, the freeze-dried peptides contained 5 to 10% moisture by weight. Stock solutions, typically 50 mM, were freshly prepared in $D_2O$ from: $NiCl_2 \cdot 6H_2O$; $K_2[PdCl_4]$ anhydrous; $K_2[PtCl_4]$ anhydrous; and $Na[AuCl_4] \cdot 2H_2O$. The addition of metal ions to the octarepeat peptides was performed using small aliquots of these stock solutions. The pH was measured both before and after each spectrum was recorded. The uncorrected meter reading in $D_2O$ is indicated as pH* throughout. Adjustments of pH were made either by the addition of small aliquots of 10 mM NaOD, and DCl or by the use of deuterated phosphate buffer, typically 20–50 mM.

### Absorption spectroscopy (UV/Vis) and circular dichroism (CD)

UV/Vis electronic absorption spectra were obtained with a Hitachi U-3010 double beam spectrophotometer using a 1 cm path length. CD spectra were recorded on an AVIV instrument at 25 °C using a 0.1 cm path length cell for spectra recorded between 185 and 260 nm (far-UV region) and a 1 cm path-length cell for data between 260 and 800 nm (near-UV and visible region) as previously described.[16,12]

### Nuclear magnetic resonance spectroscopy

NMR spectra were acquired on either a Bruker Avance 600 MHz spectrometer equipped with a 5 mm triple resonance inverse-detection triple-resonance ($^1$H, $^{13}$C, $^{15}$N) *z*-gradient probe, or a Bruker AMX 400 MHz spectrometer with a proton dedicated 5 mm probe. 2D homo-nuclear DQF-COSY, NOESY, TOCSY and ROESY ($\tau_{mixing} = 300$ ms) spectra were recorded with typically 4096 by 512 data points. Spectra were collected over 9216 Hz (15 ppm) spectral widths in both dimensions. States-TPPI was used for quadrature detection. Spectra were zero-filled to 2048 real points in f1, and a $\pi/2$ shifted, squared sine-bell window function applied prior to Fourier transformation. The Pd–QPHGGGWGQ spectra were acquired in 90%/10% $H_2O/D_2O$ at 303 K. Water suppression was achieved using WATERGATE.[51] $^1$H spectra were

 

referenced to the water peak.[52] In addition, $^{13}$C-HSQC spectra were acquired for the Pd–QPHGGGWGQ complex, 1 mM peptide concentration was sufficient for natural abundance measurements. Spectral widths of 14 ppm $^{1}$H by 100 ppm $^{13}$C were recorded with 2048 by 256 complex points. The spectra were transformed with a squared cosine function. Data were processed using XWINNMR (Bruker). Proton NMR assignments were achieved using standard homo-nuclear 2D methods.[53]

### NMR structure calculations

Peak volumes in the ROESY spectra were classified as strong, medium and weak, corresponding to upper bounds of 3.0 Å, 5.0 Å and 6.0 Å. Intensities were calibrated by comparison to intra-residue ROEs between fixed proton distances of the tryptophan ring. The lower distance boundary was set at 1.8 Å for all classes. Pseudoatom corrections were applied where necessary. Stereo-specific assignments for His ββ′ and Trp ββ′ AMX systems were not possible due to spectral overlap nor were Gly αα′ stereo-specific assignments made. No metal-to-ligand restraints were assumed for structure calculation.

Structures were determined using torsion angle dynamics with simulated annealing in XPLOR.[54] In the first step, an *ab initio*, torsion angle dynamics protocol was used starting from an extended conformation having random $\phi$ and $\psi$ angles. Fifty structures were produced after 45 ps of high temperature dynamics, followed by cooling over 45 ps and, finally, 200 steps of energy minimisation. Structures corresponding favourably to the experimental restraints were refined by 3000 steps of Powell minimisation under the influence of a full force field based on CHARM parameters.[55] The 20 lowest energy structures were chosen to represent the solution structure of Pd–QPHGGGWGQ. Acceptance criteria were no NOE violation >0.5 Å. Structural analysis was performed using PROCHECK-NMR.[56]

## Results

### $^{1}$H NMR monitored kinetics of $Pd^{2+}$ binding to PrP octarepeat fragments

The reaction of HGGGW with $Pd^{2+}$ was monitored by 1D $^{1}$H NMR, over a period of 12 hours, during which time spectra were obtained at hourly intervals. Fig. 1 shows the evolution of $^{1}$H NMR signals in the aromatic region after the addition of 0.5 mole equivalent $Pd^{2+}$ to HGGGW at pH* 8.5. Initially, overlapping sets of new $^{1}$H NMR lines are seen and after 1 hour the proton spectrum still has the appearance of multiple sets of overlapping lines. Subsequent spectra show an increase in the intensity of a number of resonances, accompanied by the diminution of other signals and a reduction in complexity. After 12 hours two distinct sets of lines of similar intensity are resolved. One set of lines is assigned to apo HGGGW while the other set is assigned to the Pd–HGGGW complex. The presence of two sets of NMR signals indicates a slow-exchange complex on the NMR chemical-shift time scale. Where individual lines are resolved there is no significant change in half-height line-width between the apo spectra and the $Pd^{2+}$ loaded spectra. The ratio of the two sets of resonances is approximately 1 : 1, at 0.5 mole equivalent $Pd^{2+}$, indicating the formation of a diamagnetic peptide–metal complex

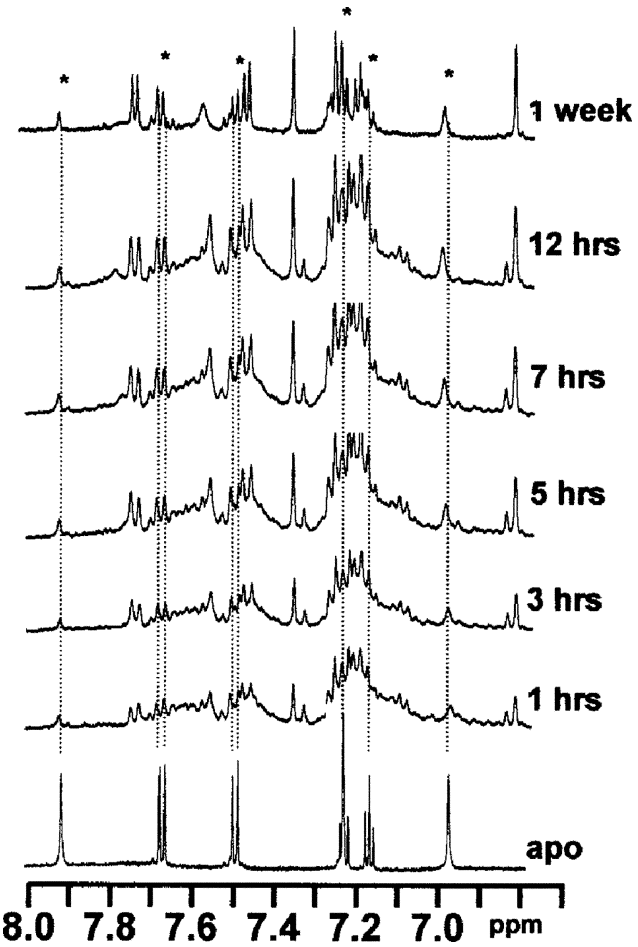


**Fig. 1** $^{1}$H NMR monitored reaction kinetics of $Pd^{2+}$ binding to HGGGW. 1 mM HGGGW reacted with 0.5 mole equivalent of $Pd^{2+}$ at pH* 8.5 in $D_2O$. Spectra were recorded at 400 MHz, 303 K at hourly intervals up to 12 hours. The aromatic region is shown. A final $^{1}$H NMR spectrum was recorded after 1 week at 600 MHz. Signals for apo HGGGW (indicated by *) and $Pd^{2+}$ bound HGGGW are observed in a 1 : 1 ratio.

with 1 : 1 stoichiometry. In Fig. 1, the spectrum of Pd–HGGGW, one week post $Pd^{2+}$ ion addition, shows that the two sets of signals have become still more distinct. It is clear from the $^{1}$H NMR spectra that after addition of $Pd^{2+}$ ions multiple species form rapidly in ~5 minutes or less and a single Pd–peptide complex then evolves over a period of 24 hours.

The Pd–HGGGW reaction kinetics were also studied in a phosphate buffered system at pH* 7.6 and similar behavior was observed. Fig. 2 shows a comparison between the reaction kinetics of the pH* 8.5 unbuffered and the pH* 7.6 phosphate-buffered systems. The signal intensity of the resonances from the palladium complex is shown plotted *versus* time. For this the mean of the peak heights of the histidine C4H and tryptophan C2H lines were used. No significant difference is seen in reaction kinetics between pH* 7.6 and pH* 8.5 either with or without phosphate buffer. In both cases the half-maximum signal is reached at ~3 hours at 30 °C.

After 1 week the line widths at half-height of singlet NMR signals from the Pd–HGGGW complex were typically 3.3 Hz. These line widths are consistent with a monomeric Pd–HGGGW species. Some precipitate was visible at this stage and so it is likely

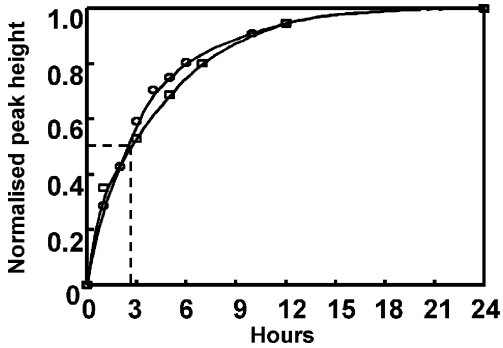


**Fig. 2** $^{1}$H NMR peak intensities monitored with time for $Pd^{2+}$ binding to HGGGW. HGGGW (1 mM) reacted with 0.5 mole equivalents of $Pd^{2+}$ at pH* 8.5, non-buffered (*open box*) or in 20 mM deuterated phosphate buffer at pH* 7.6 (*open circle*). In each case the sum of the peak heights of the histidine 4H and tryptophan 2H signals are plotted *versus* time post $Pd^{2+}$ addition. The sum of the peak heights are normalized to 1.0 at maximal intensity after 24 hours. The time taken to reach half-maximum signal is shown as ~3 hours under both conditions.

that some of the changes in the spectra reflect the removal from solution of minor polymeric species due to precipitation.

### Stoichiometry of $Pd^{2+}$–PrP octarepeat complexes by $^{1}$H NMR

Fig. 3 shows the titration of separate samples of HGGGW with varying amounts of $Pd^{2+}$ at pH* 7.6 in phosphate buffer examined by $^{1}$H NMR 24 hours post $Pd^{2+}$ addition. Increasing addition of $Pd^{2+}$ causes a diminution of the apo HGGGW NMR signals and the appearance of a new set of signals. Upon the addition of 1 mole equivalent $Pd^{2+}$ only the NMR signals from the $Pd^{2+}$ bound form were observed, indicating tight binding at 1 mM peptide concentrations.

Similar behavior was observed for the titration of HGGG with $Pd^{2+}$. Two sets of $^{1}$H NMR signals were produced for the apo and $Pd^{2+}$ bound peptide (data not shown) consistent with 1 : 1 peptide metal complex formation. For example, the signals for the apo and the $Pd^{2+}$ bound species from the histidine resonances were of equal intensity at 0.5 mole equivalent of $Pd^{2+}$. At 1 mole equivalent of $Pd^{2+}$ there was only one set of signals for the $Pd^{2+}$ bound His C2H and His C4H resonances.

Fig. 4 shows the $Pd^{2+}$ titration of QPHGGGWGQ. The apopeptide signals decrease with $Pd^{2+}$ addition, by one mole equivalent of $Pd^{2+}$ one major species is present. Fig. 5 shows the intensities of a number of well resolved residues plotted *versus* $Pd^{2+}$ addition to QPHGGGWGQ. As the titration progresses beyond 1 mole equivalent $Pd^{2+}$ the metal complex tryptophan C4H signal becomes progressively diminished while, simultaneously, a new doublet signal can be observed at 7.90 ppm. Similarly, the metal complex histidine εH signal becomes progressively diminished as the titration progresses beyond 1 mole equivalent $Pd^{2+}$, while a new line appears at 8.39 ppm. Thus, with the addition of 2 mole equivalents of $Pd^{2+}$ there are two $Pd^{2+}$ complex species in evidence. The second species becomes even more evident at higher additions of $Pd^{2+}$ suggesting an alternative-binding mode at elevated $Pd^{2+}$ levels.

In summary, as with $Cu^{2+}$ binding to HGGG, HGGGW and QPHGGGWGQ,[13,12] $Pd^{2+}$ binds to the PrP fragments in a 1 : 1 ratio. This suggests that $Pd^{2+}$ might be useful as a diamagnetic mimic of $Cu^{2+}$ binding.

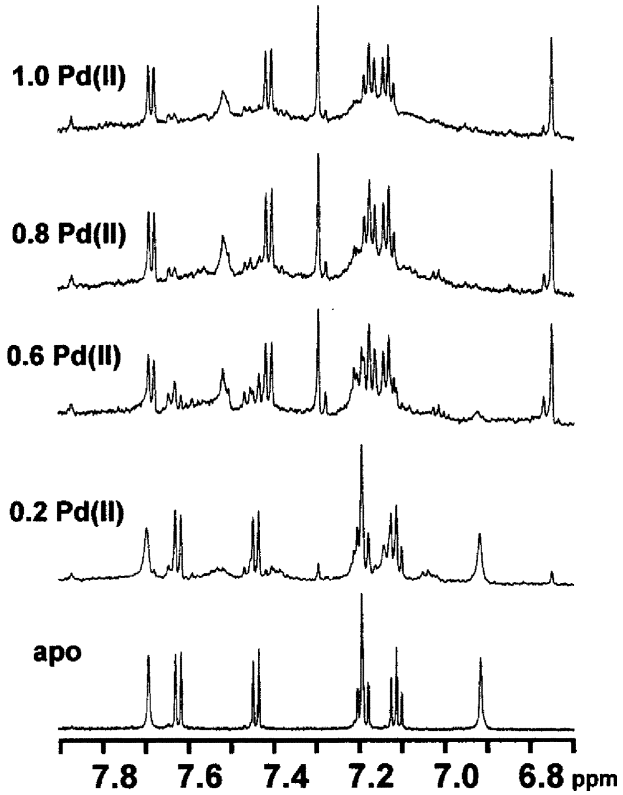


**Fig. 3** $^{1}$H NMR spectrum of HGGGW titrated with $Pd^{2+}$. Pd–HGGGW samples were prepared 24 hours before spectra acquisition in 20 mM deuterated phosphate buffer at pH* 7.6. $Pd^{2+}$ additions are shown as mole equivalents. 600 MHz spectra were acquired at 303 K. The 0.2, 0.6 and 0.8 mole equivalent spectra are scaled by 2× relative to apo, and the 1.0 mol equivalent $Pd^{2+}$ spectrum scaled by 3× to allow for the loss of sample due to precipitation with increasing $Pd^{2+}$ additions.

### $^{1}$H and $^{13}$Cα NMR assignments and $Pd^{2+}$ induced co-ordination shifts

A suite of $^{1}$H homo-nuclear DQF-COSY, TOCSY, NOESY and ROESY spectra were obtained for apo peptides and peptide–$Pd^{2+}$ complexes. Resonance assignments were made using the standard homo-nuclear 2D methodology.[53] Generally, the 2D NOESY spectra produced a limited number of weak cross-peaks for all three Pd bound peptides. The cross peaks obtained with the peptides, HGGG and HGGGW, were of the opposite sign to the diagonal, as is typical for small molecules, while QPHGGGWGQ cross peaks gave the same sign as the diagonal. It was considered likely that the correlation times of the peptides fall within the range over which the NOE tends towards a null, between the small molecule and macromolecular regimes. In contrast, the ROESY spectrum of QPHGGGWGQ with 1 mole equivalent $Pd^{2+}$ using 300 ms mixing time, gave a reasonable number of both intra- and inter-residue ROEs. Fig. 6 shows TOCSY and ROESY spectra for Pd–QPHGGGWGQ. Table 1 shows the $^{1}$H chemical shift assignments of apo and $Pd^{2+}$ bound QPHGGGWGQ, HGGG and HGGGW peptides. The apo peptide $^{1}$H resonance assignments at pH* 7.6 are close to the values published for random coil

 

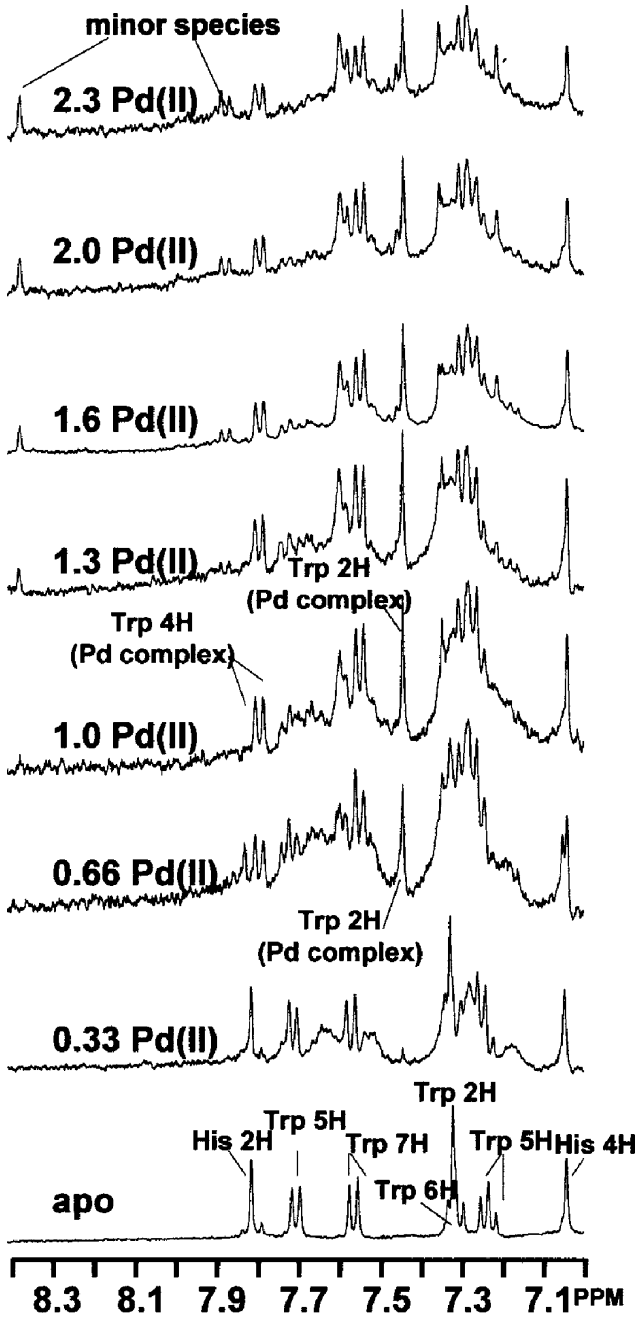


**Fig. 4** $^{1}$H NMR spectrum of QPHGGGWGQ titrated with $Pd^{2+}$. Pd–QPHGGGWGQ samples (1 mM, 20 mM deuterated phosphate buffer at pH* 7.6) were prepared 24 hours prior to acquisition. $Pd^{2+}$ additions are shown as mole equivalents. 400 MHz spectra were acquired at 303 K.

resonances.[53] In addition, a natural abundance $^{1}$H–$^{13}$C HSQC spectrum was used to obtain $^{13}$C Cα co-ordination shifts upon $Pd^{2+}$ binding to QPHGGGWGQ, presented in Table 2.

The TOCSY spectrum (in 90% $H_2O$) shown in Fig. 6 indicates that amide protons (NH–αH connectivities) are observable for Glu1, His3, and Trp7 to Glu9 but Gly5 and Gly6 amide main chain protons are not observed in the $Pd^{2+}$ bound proton TOCSY spectra. Metal co-ordination to main-chain nitrogens is expected to displace the amide protons, hence their absence suggests that $Pd^{2+}$ is bound to the Gly5 and Gly6 amide nitrogens.

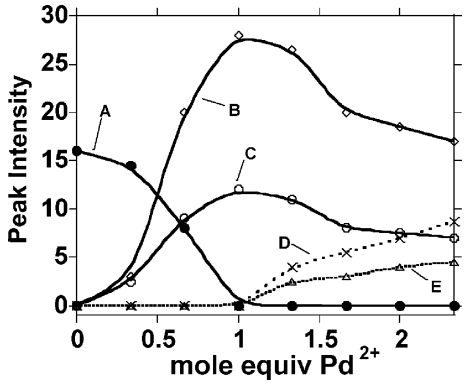


**Fig. 5** $Pd^{2+}$ binding curves for QPHGGGWGQ. $^{1}$H NMR absolute peak heights are taken from data presented in Fig. 4. Peak assignments as follows: (A) Histidine 2H; (ε) apo peptide; (B) major $Pd^{2+}$ complex tryptophan 2H; (C) major $Pd^{2+}$ complex Trp 4H; (D) minor $Pd^{2+}$ complex His 2H; (E) minor $Pd^{2+}$ complex Trp 4H.

Chemical shift changes upon $Pd^{2+}$ co-ordination can indicate the ligands directly involved in co-ordination to the metal ion, although indirect effects from the ring-current of Trp or His rings may also cause significant changes in chemical shift upon metal chelation. $^{13}$Cα co-ordination shifts on $Pd^{2+}$ binding are presented in Table 2. Upon $Pd^{2+}$ co-ordination all residues, with the exception of the two glutamine residues (which are outside of the binding motif), display high-field shifts of the Cα resonances. The most significant Cα high-field shifts are those of Gly5 and Gly6 (17.7 and 10.7 ppm respectively). The high-field shift of these Cα resonances suggests that $Pd^{2+}$ co-ordination occurs to the adjacent amide nitrogen of these residues. This assertion is supported by the observed displacement of the Gly5 and Gly6 amide protons upon $Pd^{2+}$ co-ordination.

The changes in $^{1}$H NMR chemical shifts upon co-ordination of $Pd^{2+}$ may be compared to those observed for other square-planar $Pd^{2+}$ complexes such as Gly-Gly-His[49] for which there is a crystal structure. Chemical shifts for the $Pd^{2+}$ bound imidazole 2H (ε) and 4H (δ) protons of 7.62 ppm and 6.96 ppm, reported here for Pd–HGGG (Table 1), are very similar to those reported for the square-planar $Pd^{2+}$ complex of GGH, 7.60 ppm and 6.97 ppm respectively.[49] However, $Pd^{2+}$ co-ordinates to the δN in the crystal structure of Pd-GlyGlyHis while we show $Pd^{2+}$ co-ordination is most likely to be to the εN in the octarepeat complex. Co-ordination shifts to high-field are typically observed for the α protons of residues in which the main-chain amide co-ordinates the metal ion. For example, the Pd–GGH complex produces co-ordination shifts for α protons of −0.23; −0.09; −0.19 ppm respectively,[49] see also ref. 57. Similarly, Hα protons in HGGG exhibit high-field shifts upon $Pd^{2+}$ co-ordination. However, the $Pd^{2+}$ co-ordination shifts are relatively small and could be, for example, masked by quite modest ring-current effects. For this reason, inferences about co-ordinating ligands in $Pd^{2+}$ complexes based on chemical shifts alone many not be valid.

Table 3 compares the $Pd^{2+}$ bound $^{1}$H chemical shifts for HGGG, HGGGW and QPHGGGWGQ in order to investigate the effect of the presence of tryptophan on the Pd–HGGG complex. In general, the differences between HGGGW and QPHGGGWGQ are small, for example the difference in chemical shift for the His

**Table 1** $^{1}$H Chemical shift (ppm) for apo and $Pd^{2+}$ bound octarepeat peptide fragments. Data for three peptide fragments are shown, QPHGGGWGQ, HGGGW and HGGG. The difference in chemical shift between apo and $Pd^{2+}$ peptide is also indicated

| | | QPHGGGWGQ | | | HGGGW | | | HGGG | | |
|---|---|---|---|---|---|---|---|---|---|---|
| Residue | | Apo | Pd bound | δ Pd − δ apo | Apo | Pd bound | δ Pd − δ apo | Apo | Pd bound | δ Pd − δ apo |
| Q1 | NH | 8.23 | 8.30 | +0.07 | | | | | | |
| | α | 4.61 | 4.61 | 0.00 | | | | | | |
| | β | 2.04 | 1.97 | −0.07 | | | | | | |
| | β′ | 1.86 | 2.15 | +0.29 | | | | | | |
| | γ | 2.36 | 2.45 | +0.09 | | | | | | |
| | γ′ | 2.36 | 2.45 | +0.09 | | | | | | |
| P2 | α | 4.37 | 4.27 | −0.10 | | | | | | |
| | β | 2.22 | 2.21 | −0.01 | | | | | | |
| | β′ | 1.92 | 1.92 | 0.00 | | | | | | |
| | γ | 1.79 | 1.98 | +0.19 | | | | | | |
| | γ′ | 1.79 | 1.98 | +0.19 | | | | | | |
| | δ | 3.75 | 3.78 | +0.03 | | | | | | |
| | δ′ | 3.59 | 3.65 | +0.06 | | | | | | |
| H3 | NH | 8.42 | 7.69 | −0.73 | | | | | | |
| | α | 4.56 | 4.25 | −0.31 | 4.56 | 4.26 | −0.30 | 4.63 | 4.48 | −0.15 |
| | β | 3.15 | 2.6 | −0.55 | 3.08 | 2.51 | −0.57 | 3.10 | 3.56 | +0.46 |
| | β′ | 3.10 | 2.6 | −0.50 | 3.00 | 2.30 | −0.70 | 3.05 | 3.11 | +0.06 |
| | 2H(ε) | 8.12 | 7.49 | −0.63 | 7.74 | 7.58 | −0.16 | 7.80 | 7.62 | −0.18 |
| | 4H(δ) | 7.07 | 6.96 | −0.11 | 6.96 | 6.81 | −0.15 | 7.03 | 6.96 | −0.07 |
| G4 | NH | 8.28 | 7.66 | 0.62 | # | # | # | # | # | # |
| | α | 4.01 | 3.99 | # | 3.87 | 4.10 | # | 4.03 | 4.21 | # |
| | α′ | 3.87 | 3.87 | # | 3.71 | 3.77 | # | 3.93 | 3.94 | # |
| G5 | NH | 8.28 | n/a | n/a | | | | | | |
| | α | 4.01 | 4.10 | # | 3.87 | 4.01 | # | 4.03 | 4.01 | # |
| | α′ | 3.87 | 3.78 | # | 3.71 | 3.69 | # | 3.93 | 3.84 | # |
| G6 | NH | 8.28 | n/a | n/a | | | | | | |
| | α | 4.01 | 4.05 | # | 3.87 | 3.84 | # | 4.03 | 3.78 | # |
| | α′ | 3.87 | 3.81 | # | 3.71 | 3.34 | # | 3.93 | 3.54 | # |
| W7 | NH | 8.05 | 7.84 | # | # | # | # | | | |
| | α | 4.66 | 4.55 | −0.11 | 4.64 | 4.50 | −0.14 | | | |
| | β | 3.32 | 3.43 | +0.11 | 3.33 | 3.49 | −0.16 | | | |
| | β′ | 3.24 | 3.35 | +0.13 | 3.21 | 2.39 | +0.18 | | | |
| | 2H | 7.24 | 7.35 | +0.11 | 7.24 | 7.36 | +0.12 | | | |
| | 4H | 7.62 | 7.70 | +0.08 | 7.77 | 7.71 | −0.06 | | | |
| | 5H | 7.15 | 7.18 | +0.03 | 7.16 | 7.18 | +0.02 | | | |
| | 6H | 7.23 | 7.21 | −0.02 | 7.24 | 7.23 | −0.01 | | | |
| | 7H | 7.48 | 7.46 | −0.02 | 7.50 | 7.53 | +0.03 | | | |
| G8 | NH | 8.30 | 8.49 | +0.19 | | | | | | |
| | α | 3.87 | 4.21 | +0.34 | | | | | | |
| | α′ | 3.78 | 3.71 | −0.07 | | | | | | |
| Q9 | NH | 8.03 | 8.10 | +0.07 | | | | | | |
| | α | 4.27 | 4.29 | +0.02 | | | | | | |
| | β | 2.15 | 1.97 | −0.18 | | | | | | |
| | β′ | 1.92 | 2.18 | +0.26 | | | | | | |
| | γ | 2.34 | 2.31 | −0.03 | | | | | | |
| | γ′ | 2.34 | 2.31 | −0.03 | | | | | | |

**Table 2** $^{13}$Cα chemical shifts for apo and $Pd^{2+}$ bound QPHGGGWGQ octarepeat. Chemical shifts are in ppm. The difference in chemical shift upon $Pd^{2+}$ co-ordination is also indicated

| | $^{13}C^{\alpha}$ apo | $^{13}C^{\alpha}$ $Pd^{2+}$ | $^{13}C^{\alpha}$ Difference |
|---|---|---|---|
| Q1 | | | |
| P2 | 61.5 | 63.2 | +1.7 |
| H3 | 52.0 | 57.0 | +5.0 |
| G4 | 43.3 | 44.5 | +1.2 |
| G5 | 43.3 | 61.0 | +17.7 |
| G6 | 43.3 | 54.0 | +10.7 |
| W7 | 56.5 | 57.0 | +0.5 |
| G8 | 42.0 | 44.6 | +2.6 |
| Q9 | 54.6 | 53.0 | +1.6 |

Hα resonance between Pd–QPHGGGWGQ and Pd–HGGGW is only −0.01 ppm. Similarly the Trp resonances are largely unaffected, suggesting that the presence of the other residues present in QPHGGGWGQ have little effect on the co-ordination geometry. In contrast, the difference in His Hα and Hβ chemical shifts between Pd–HGGG and Pd–HGGGW are relatively large; −0.22 ppm, (His Hα) −0.60 ppm and −1.26 ppm (His Hββ′). The inclusion of the Trp side chain in HGGGW causes a pronounced high-field shift of the His Hα and Hβ resonances, presumably due to the ring current effects caused by the close proximity of the ring face of the tryptophan.

### NMR solution structure of $Pd^{2+}$–QPHGGGWGQ

Analysis of the $Pd^{2+}$ loaded 300 ms ROESY spectrum yielded a total of 71 distance restraints used in the structural calculations. Of these, 21 are medium or long-range restraints, and are summarised

 

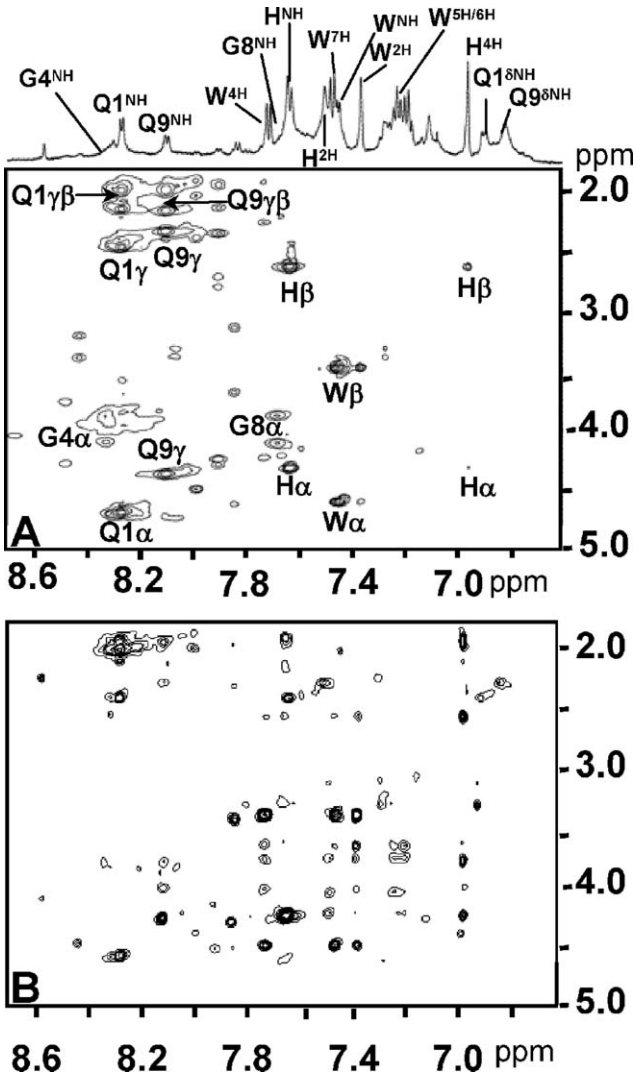


**Fig. 6** 2D TOCSY and ROESY NMR spectra for Pd–QPHGGGWGQ complex. Assigned resonances are labeled in both the TOCSY spectrum (A) and the corresponding 1D spectrum. The ROESY spectrum (B), shows that a number of sequential and longer range ROE cross peaks are observed. Both are 600 MHz spectra recorded at 303 K, pH 6.5 in 90%/10% $H_2O/D_2O$, at 1 mM peptide concentration.

in Table 4. Metal-to-ligand restraints were not used for structure calculation in order not to pre-judge the co-ordination geometry. ROEs between the proline, tryptophan and histidine dominate the restraint file. Pro2 was determined to be in the *trans* configuration with a strong Hδ Pro2 to Hα Glu1 ROE cross-peak. Structures were obtained using restrained molecular dynamics. The lowest energy conformers chosen to represent the structure of Pd–QPHGGGWGQ have an average RMSD (with respect to the mean structure) over all residues ($Q_1$–$Q_9$) of 0.58 Å for the main-chain and 0.97 Å for all heavy atoms. Procheck-NMR was used to analyse the structures[56] and it was found that all residues lie in the most favoured and allowed regions of the Ramachandran plot. The structural statistics are given in Table 4. None of the structures had NOE violations > 0.2 Å. Fig. 7 shows the family of conformers describing the solution structure of QPHGGGWGQ with $Pd^{2+}$ bound.

**Table 3** A comparison of $^1$H NMR chemical shift for Pd–HGGG, Pd–HGGGW and Pd–QPHGGGWGQ. Difference in chemical shift (in ppm) between Pd–HGGGW and Pd–HGGG and also chemical shift differences between Pd–QPHGGGWGQ and Pd–HGGGW are shown. Only His and Trp resonances are shown due to a lack of stereo-specific assignments for glycine resonances

| Resonance | HGGGW–HGGG (ppm) | QPHGGGWGQ–HGGGW (ppm) |
|---|---|---|
| Histidine | | |
| Hα | −0.22 | −0.01 |
| Hβ | −0.60 | +0.09 |
| Hβ′ | −1.26 | +0.30 |
| 2H(ε) | −0.04 | −0.09 |
| 4H(δ) | −0.15 | +0.15 |
| Tryptophan | | |
| Hα | [a] | +0.02 |
| Hβ | [a] | +0.03 |
| Hβ′ | [a] | +0.02 |
| 2H | [a] | +0.01 |
| 4H | [a] | +0.03 |
| 5H | [a] | 0.00 |
| 6H | [a] | +0.01 |
| 7H | [a] | +0.02 |

[a] Not applicable.

It is clear from the ensemble that $Pd^{2+}$ chelation causes the main-chain to form an ordered loop around the metal ion. In particular the $Pd^{2+}$ co-ordinating residues, HGGGW, give a RMSD of 0.30 Å for the main-chain. Once the family of structures was obtained the probable position of the $Pd^{2+}$ ion was modeled into the loop that contains residues HGGGW. Typical palladium to nitrogen (or oxygen) bond lengths for a square-planar complex are 2.0 Å.[49] Only $Pd^{2+}$ co-ordination to the His3 side chain Nε, Gly5 amide N and Gly6 amide N, produced a complex that did not violate any of the ROEs, and retained the conformation determined in the absence of metal restraints. In particular, the relative position of the imidazole ring to other potential ligands did not lend itself to co-ordination of $Pd^{2+}$ to the His δ nitrogen. The identity of the fourth ligand is not readily apparent from the family of structures suggesting water as a fourth ligand. A possible alterative candidate is the Trp amide, however this appears to be too distant. The Gly6 carbonyl oxygen appears to be ruled out on the grounds of bond angle geometry.

Obtaining a well-defined NMR structure for this small peptide is fraught with difficulties. The number of long-range distance restraints is limited in a 9-residue peptide. The presence of four glycine residues and the loss of amide protons due to metal co-ordination reduce the number of observable NOEs still further. Despite these difficulties His Nε, Gly5 Nα and Gly6 Nα are the only set of co-ordinating ligands that can be incorporated into the solution structure without significant rearrangement of the structure and the introduction of a number of ROE violations. In addition, the determined solution structure, and the inferred position of the $Pd^{2+}$ ion, is consistent with the loss of main-chain amide protons observed for Gly5 and Gly6 upon $Pd^{2+}$ addition. Furthermore, the $^{13}$Cα co-ordination shift data also suggest that QPHGGGWGQ co-ordinates the $Pd^{2+}$ ion by the histidine side-chain and two glycine residues; Gly5 and Gly6. Finally, the relative orientation of the tryptophan side-chain, in the proposed solution structure, is consistent with the $^1$H co-ordination shifts (Table 3).

**Table 4** Structural and energy statistics for $Pd^{2+}$ loaded QPHGGGWGQ

| | |
|---|---|
| (A) *Experimental constraints*[a] | |
| Intra-residue distance | 20 |
| Sequential distances ($\|i–j\| = 1$) | 30 |
| Medium range distances ($\|i–j\| = < 5$) | 13 |
| Long range distance ($\|i–j\| = > 5$) | 8 |
| Dihedral angles | 0 |
| (B) *Constraint violations* | |
| Number of NOE violations > 0.2 Å | 0 |
| Maximum NOE violation/Å | 0.196 |
| (C) *RMS deviation from experimental constraints* | |
| NOE/Å | $3.3 \times 10^{-2} \pm 6.59 \times 10^{-3}$ |
| (D) *RMS deviation from idealised geometry* | |
| Bonds/Å | $4.14 \times 10^{-3} \pm 2.32 \times 10^{-4}$ |
| Angles/° | $6.65 \times 10^{-1} \pm 2.55 \times 10^{-2}$ |
| Impropers/° | $3.08 \times 10^{-1} \pm 1.59 \times 10^{-2}$ |
| (E) *Energies*[b]/kcal $mol^{-1}$ | |
| $E_{(NOE)}$ | $1.72 \pm 0.66$ |
| $E_{(Van\ der\ Waals)}$ | $-17.01 \pm 3.49$ |
| $E_{(total)}$ | $2.88 \pm 4.15$ |
| (F) *RMS to the average co-ordinates*/Å | |
| Backbone (N, $C^{\alpha}$, C) (1–9)[c] | 0.58 |
| Backbone (N, $C^{\alpha}$, C) (3–7)[c] | 0.30 |
| Heavy atoms (1–9)[c] | 0.97 |
| Heavy atoms (3–7)[c] | 0.59 |
| (G) *Ramachandran analysis* (1–9)[c] (%) | |
| Residues in disallowed regions | 0 |
| Residues in generously allowed regions | 0 |
| Residues in allowed regions | 52.9 |
| Residues in most favourable regions | 47.1 |

[a] $Pd^{2+}$ to ligand restraints have not been used in structure calculations. [b] Energy calculated with the CHARM M19 empirical energy function. [c] Residues included in analysis are indicated in parentheses.

In particular, the Trp indole ring is orientated face-on to the His β protons, thus accounting for the large (−1.26 ppm and −0.60 ppm) high-field co-ordination shifts observed.

Despite the success in obtaining $^1$H NMR spectra with $Pd^{2+}$ bound to a single octarepeat, suitable for solution structure determination, attempts to obtain usable $^1$H NMR spectra of multiple octarepeats bound to $Pd^{2+}$ have, to date, been unsuccessful. The addition of various amounts of $Pd^{2+}$, to the two and four octarepeat fragment, over a range of concentrations and pH values, caused immediate turbidity and precipitation. Only broad $^1$H NMR signals, characteristic of polymerised species, were observed.

### $Ni^{2+}$, $Pt^{2+}$ and $Au^{3+}$ will not form a square-planar complex with the octarepeats

$Ni^{2+}$ is often a good replacement ion for square-planar type II $Cu^{2+}$ binding. For example, $Ni^{2+}$ binding to the $Cu^{2+}$ binding site of serum albumin[57,46] and more recently to the amyloidgenic region of PrP, centered at residues His111 and His96,[16] have been reported. $^1$H NMR spectra of HGGGW loaded with increasing amounts of $Ni^{2+}$ were obtained. However, surprisingly there was no evidence of a low-spin, diamagnetic, square-planar $Ni^{2+}$ complex. Neither were shifts in resonances observed, that would imply a diamagnetic complex in fast exchange. Instead the incremental addition of $Ni^{2+}$ ions caused increased broadening of all the NMR signals present, suggesting the formation of a paramagnetic, high spin, tetrahedral or octahedral complex. Similar observations were made with the two octarepeat peptide, PrP(2octa). Although various mole equivalents of $Ni^{2+}$ were studied over a range of pH values (between pH 6 to 11) no evidence of the formation of a diamagnetic Ni-complex species was observed. Furthermore, in agreement with the $^1$H NMR data, d–d absorption bands or visible CD bands between 420–450 nm, characteristic of a $Ni^{2+}$ square-planar complex,[45,16,47] were not observed.

Like $Ni^{2+}$, $Pt^{2+}$ can replace $Cu^{2+}$ to form square-planar complexes. Proton NMR spectra were obtained for HGGGW titrated with $PtCl_2$. The addition of increasing amounts of $Pt^{2+}$ caused progressive broadening of histidine 2H (ε) and 4H (δ) resonances (data not shown). Again there was no observation of $^1$H NMR resonances that would indicate a monomeric Pt–HGGGW complex in slow-exchange.

$Au^{3+}$ is known to form complexes with square-planar geometry.[49] Additions of $Au^{3+}$ were monitored by absorption spectroscopy. An absorption band at 520 nm was observed to evolve with $Au^{3+}$ addition. The observation of a strong purple colour on the addition of $Au^{3+}$ to the peptide could be misinterpreted as the formation of an $Au^{3+}$–peptide complex. However it is clear that the band at 520 nm is due to the presence of colloidal Au(0) rather than Au–HGGGW complex formation. Au(0) colloids have previously been reported to produce a band around 520 nm depending on particle size.[58] Reduction of $Au^{3+}$ in solutions exposed to ambient light has been reported and ligand oxidation has been reported in the reaction of $NH_3$–Gly–Gly–His with $Au^{3+}$.[49] For these reasons it was concluded that $Au^{3+}$ would not be of use as a probe of $Cu^{2+}$ binding to the octarepeats.

## Discussion

There are relatively few reports of $Pd^{2+}$ peptide complexes, however $Pd^{2+}$ can substitute for $Cu^{2+}$ in square-planar complexes. For

 

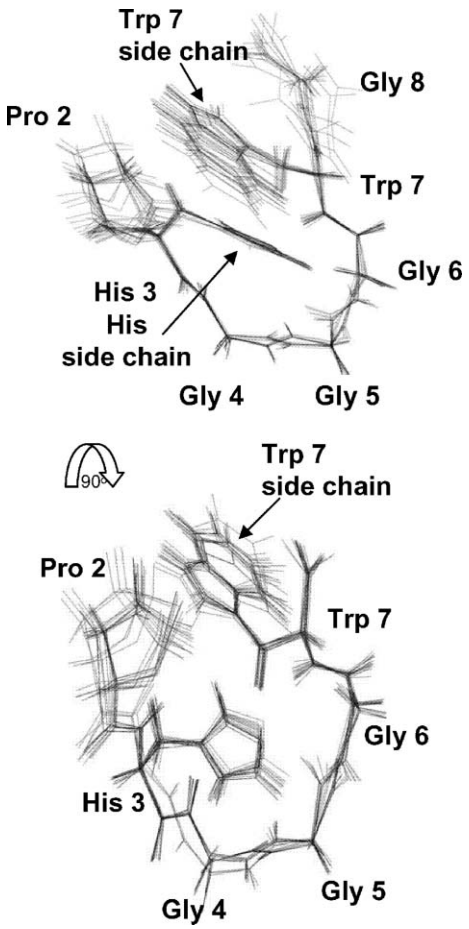


**Fig. 7** Solution structure of $Pd^{2+}$ bound QPHGGGWGQ. An ensemble of the lowest energy backbone conformers. The backbone ensemble is also shown rotated by 90°. Structures are calculated without the use of Pd to ligand restraints. The most plausible co-ordination of the $Pd^{2+}$ ion is to the His3 Nδ, Gly5 Nα and Gly6 Nα. $Pd^{2+}$ chelation causes the peptide to form a loop conformation around the metal ion. Main-chain RMSD for the metal binding motif, Pd–HGGGW, is 0.30 Å.

example, $Pd^{2+}$ is square-planar when bound to Gly-Gly-His[49] and to Gly-His-Lys.[59] Here, $^1$H NMR investigations have shown that $Pd^{2+}$ will also bind to HGGG, HGGGW and QPHGGGWGQ, forming 1 : 1 diamagnetic complexes in slow-exchange on the NMR timescale, between free and $Pd^{2+}$ bound peptide. The formation of the $Pd^{2+}$ complexes is slow reaching half maximal signal only after ~3 hours. The end-point complexes are stable at 25 °C over a number of weeks. The relatively slow formation of the palladium complex is not unprecedented, similar kinetics have been reported for the formation of $Ni^{2+}$, $Pd^{2+}$ and $Pt^{2+}$ complexes.[47] The reaction of $Pd^{2+}$ with Gly-His-Lys has been shown to proceed to a single product over 10 hours[59] and a similar time scale has been reported for the reaction of Gly-Gly-His with $Pd^{2+}$.[49] The rate limiting step in the formation of the Pd–HGGGW complex may be the ionisation of amide hydrogen atoms, as has been observed for $Ni^{2+}$–peptide complexes.[47]

Although $Pd^{2+}$ forms a square-planar complex with the single octarepeat peptide it is apparent from the NMR structure that the co-ordination geometry is not the same as found in the $Cu^{2+}$ bound HGGGW crystal structure.[14] In the crystal structure $Cu^{2+}$ is co-ordinated by the His3 side chain Nδ, Gly4 amide N and Gly5 amide N and carbonyl O of Gly5. An axially co-ordinated water molecule is also observed.[14] In contrast, the most probable ligands for the $Pd^{2+}$ co-ordination, based on the NMR data, include the His3 side chain Nε, Gly5 amide nitrogen and Gly6 amide nitrogen. The $Cu^{2+}$ complex forms a seven membered ring between Gly 4 Hα and His Nδ and it is possible that this configuration is too strained with the inclusion of the $Pd^{2+}$ ion, forcing the very different $Pd^{2+}$ co-ordination observed.

$Ni^{2+}$ often forms diamagnetic, low-spin, square-planar complexes with histidine containing peptides.[47,16] Surprisingly in the case of the PrP ocatrepeats no such $Ni^{2+}$ complex is formed. $Cu^{2+}$ and $Ni^{2+}$ ions have the ability to co-ordinate to histidine imidazole nitrogens. Using the histidine as an 'anchor', $Cu^{2+}$ and $Ni^{2+}$ ions are capable of deprotonating neighbouring amide main-chain nitrogens in unstructured regions of proteins.[47] $Cu^{2+}$ can do this at physiological pH values, but $Ni^{2+}$ requires elevated pH's (between pH 8 and 9) to achieve deprotonation of main-chain amides. This has been observed for $Ni^{2+}$ binding to His96 and His111 in the unstructured amyloidogenic region of $PrP^C$.[16] However, $Ni^{2+}$ co-ordination in a square-planar geometry to the octarepeat peptide does not take place even at elevated pH values. Both $Cu^{2+}$ and $Ni^{2+}$ prefer to co-ordinate to amide nitrogen atoms that are to the N-terminus of the histidine residues. This results in the formation of a more stable six membered chelate ring with the His δN and the main-chain αN of the histidine. Co-ordination of amides to the C-terminus of the histidine imidazole ring results in a less stable seven membered ring. In the case of the octarepeats, N-terminal co-ordination is not possible due to the presence of a proline preceding the His residue. It is perhaps the presence of proline that precludes the formation of a square-planar complex of $Ni^{2+}$, $Pt^{2+}$ or $Au^{3+}$ with the octarepeats, giving this region of the prion protein its specificity for $Cu^{2+}$ ions.

## Acknowledgements

BBSRC Project Grants. Our thanks to Dr Harold Toms for assistance with NMR experiments at Queen Mary and the MRC Biomedical NMR Centre at the NIMR, Mill Hill, London for the use of NMR facilities.

## References

1 S. B. Prusiner, *Science*, 1997, **278**, 245–251.
2 A. L. Horwich and J. S. Weissman, *Cell*, 1997, **89**, 499–510.
3 S. B. Prusiner, *Proc. Natl. Acad. Sci. USA*, 1998, **95**, 13363–13383.
4 G. Legname, I. V. Baskakov, H. O. Nguyen, D. Riesner, F. E. Cohen, S. J. DeArmond and S. B. Prusiner, *Science*, 2004, **305**, 673–676.
5 R. Riek, S. Hornemann, G. Wider, M. Billeter, R. Glockshuber and K. Wuthrich, *Nature (London)*, 1996, **382**, 180–182.
6 T. L. James, H. Liu, N. B. Ulyanov, S. Farr-Jones, H. Zhang, D. G. Donne, K. Kaneko, D. Groth, I. Mehlhorn, S. B. Prusiner and F. E. Cohen, *Proc. Natl. Acad. Sci. USA*, 1997, **94**, 10086–10091.
7 D. G. Donne, J. H. Viles, D. Groth, I. Mehlhorn, T. L. James, F. E. Cohen, S. B. Prusiner, P. E. Wright and J. H. Dyson, *Proc. Natl. Acad. Sci. USA*, 1997, **94**, 13452–13457.
8 R. Zahn, A. Liu, T. Luhrs, R. Riek, C. von Schroetter, F. Lopez Garcia, M. Billeter, L. Calzolai, G. Wider and K. Wuthrich, *Proc. Natl. Acad. Sci. USA*, 2000, **97**, 145–150.
9 J. H. Viles, D. Donne, G. Kroon, S. B. Prusiner, F. E. Cohen, H. J. Dyson and P. E. Wright, *Biochemistry*, 2001, **40**, 2743–2753.
10 R. Zahn, *J. Mol. Biol.*, 2003, **334**, 477–488.
11 J. H. Viles, F. E. Cohen, S. B. Prusiner, D. B. Goodin, P. E. Wright and J. H. Dyson, *Proc. Natl. Acad. Sci. USA*, 1999, **96**, 2042–2047.

12 A. P. Garnett and J. H. Viles, *J. Biol. Chem.*, 2003, **278**, 6795–6802.
13 E. Aronoff-Spencer, C. S. Burns, N. I. Avdievich, G. J. Gerfen, J. Peisach, W. E. Antholine, H. L. Ball, F. E. Cohen, S. B. Prusiner and G. L. Millhauser, *Biochemistry*, 2000, **39**, 13760–13771.
14 C. S. Burns, E. Aronoff-Spencer, C. M. Dunham, P. Lario, N. I. Avdievich, W. E. Antholine, M. M. Olmstead, A. Vrielink, G. J. Gerfen, J. Peisach, W. G. Scott and G. L. Millhauser, *Biochemistry*, 2002, **41**, 3991–4001.
15 C. E. Jones, S. R. Abdelraheim, D. R. Brown and J. H. Viles, *J. Biol. Chem.*, 2004, **279**, 32018–32027.
16 C. E. Jones, M. Klewpatinond, S. R. Abdelraheim, D. R. Brown and J. H. Viles, *J. Mol. Biol.*, 2005, **346**, 1393–1407.
17 D. R. Brown, K. Qin, J. W. Herms, A. Madlung, J. Manson, R. Strome, P. E. Fraser, T. Kruck, A. von Bohlen, W. Schulz-Schaeffer, A. Giese, D. Westaway and H. Kretzschmar, *Nature (London)*, 1997, **390**, 684–687.
18 P. C. Pauly and D. A. Harris, *J. Biol. Chem.*, 1998, **273**, 33107–33110.
19 W. S. Perera and N. M. Hooper, *Curr. Biol.*, 2001, **11**, 519–523.
20 C. Sunyach, A. Jen, J. Deng, K. T. Fitzgerald, Y. Frobert, J. Grassi and M. W. McCaffrey, M. R., *EMBO J.*, 2003, **22**, 3591–3601.
21 W. Rachidi, D. Vilette, P. Guiraud, M. Arlotto, J. Riondel, H. Laude, S. Lehmann and A. Favier, *J. Biol. Chem.*, 2003, **278**, 9064–9072.
22 D. J. Waggoner, B. Drisaldi, T. B. Bartnikas, R. L. Casareno, J. R. Prohaska, J. D. Gitlin and D. A. Harris, *J. Biol. Chem.*, 2000, **275**, 7455–7458.
23 B. S. Wong, T. Pan, T. Liu, R. Li, R. B. Petersen, I. M. Jones, P. Gambetti, D. R. Brown and M. S. Sy, *Biochem. Biophys. Res. Commun.*, 2000, **275**, 249–252.
24 N. Shiraishi, Y. Ohta and M. Nishikimi, *Biochem. Biophys. Res. Commun.*, 2000, **267**(1), 398–402.
25 D. R. Brown, B. S. Wong, F. Hafiz, C. Clive, S. J. Haswell and I. M. Jones, *Biochem. J.*, 1999, **344**, 1–5.
26 B. S. Wong, T. Pan, T. Liu, R. Li, P. Gambetti and M. S. Sy, *Biochem. Biophys. Res. Commun.*, 2000, **273**, 136–139.
27 D. R. Brown and A. Besinger, *Biochem. J.*, 1998, **224**, 423–429.
28 T. Cui, M. Daniels, B. S. Wong, R. Li, M. S. Sy, J. Sassoon and D. R. Brown, *Eur. J. Biochem.*, 2003, **270**, 3368–3376.
29 B. S. Wong, S. G. Chen, M. Colucci, Z. Xie, T. Pan, T. Liu, R. Li, P. Gambetti, M. S. Sy and D. R. Brown, *J. Neurochem.*, 2001, **78**, 1400–1408.
30 A. M. Thackray, R. Knight, S. J. Haswell, R. Bujdoso and D. R. Brown, *Biochem. J.*, 2002, **362**, 253–258.
31 J. D. F. Wadsworth, A. F. Hill, S. Joiner, G. S. Jackson, A. R. Clarke and J. Collinge, *Nat. Cell Biol.*, 1999, **1**, 55–59.
32 W. Rachidi, A. Mange, A. Senator, P. Guiraud, J. Riondel, M. Benboubetra, A. Favier and S. Lehmann, *J. Biol. Chem.*, 2003, **278**, 14595–14598.
33 E. Quaglio, R. Chiesa and D. A. Harris, *J. Biol. Chem.*, 2001, **276**, 11432–11438.
34 K. Qin, D. S. Yang, Y. Yang, M. A. Chishti, L. J. Meng, H. A. Kretzschmar, C. M. Yip, P. E. Fraser and D. Westaway, *J. Biol. Chem.*, 2000, **275**, 19121–19131.
35 J. R. Requena, D. Groth, G. Legname, E. R. Stadtman, S. B. Prusiner and R. L. Levine, *Proc. Natl. Acad. Sci. USA*, 2001, **98**, 7170–7175.
36 F. H. Ruiz, E. Silva and N. C. Inestrosa, *Biochem. Biophys.Res. Commun.*, 2000, **269**, 491–495.
37 E. M. Sigurdsson, D. R. Brown, M. A. Alim, H. Scholtzova, R. Carp, H. C. Meeker, F. Prelli, B. Frangione and T. Wisniewski, *J. Biol. Chem.*, 2003, **278**(47), 46199–46202.
38 D. R. Brown and H. Kozlowski, *Dalton Trans.*, 2004, 1907–1917.
39 D. R. Brown, *Brain Res. Bull.*, 2001, **55**, 165–173.
40 D. R. Brown, *Trends Neurosci.*, 2001, **24**, 85–90.
41 S. Lehmann, *Curr. Opin. Chem. Biol.*, 2002, **6**, 187–192.
42 N. Vassallo and J. Herms, *J. Neurochem.*, 2003, **86**, 538–544.
43 G. L. Millhauser, *Acc. Chem. Res.*, 2004, **37**, 79–85.
44 J. Stockel, J. Safar, A. C. Wallace, F. E. Cohen and S. B. Prusiner, *Biochemistry*, 1998, **37**, 7185–7193.
45 J. D. Glennon and B. Sarkar, *Biochem. J.*, 1982, **203**, 15–23.
46 P. J. Sadler, A. Tucker and J. H. Viles, *Eur. J. Biochem.*, 1994, **220**, 193–200.
47 H. Sigel and R. Martin, *Chem. Rev.*, 1982, **82**, 385–426.
48 M. Wienken, B. Lippert, L. Zangrando and E. Randaccio, *Inorg. Chem.*, 1992, **31**, 1983–1992.
49 S. L. Best, T. K. Chattopadhyay, M. I. Djuran, R. A. Palmer, P. J. Sadler, I. Sovago and K. Varnagy, *J. Chem. Soc., Dalton Trans.*, 1997, 2587–2596.
50 S. C. Gill and P. H. von Hippel, *Anal. Biochem.*, 1989, **182**, 319–326.
51 M. Liu, X. Mao, C. Ye, H. Huang, J. K. Nicholson and J. C. Lindon, *J. Magn. Reson.*, 1998, **132**, 125–129.
52 J. Cavanagh, W. J. Fairbrother, A. G. Palmer and N. J. Skelton, *Protein NMR spectroscopy: Principles and practice*, Academic Press, San Diego, CA, 1996.
53 K. Wuthrich, *NMR of Proteins and Nucleic Acids*, Wiley, New York, 1986.
54 A. T. Brunger, *X-PLOR Version 3.1 A System for X-ray Crystallography and NMR*, Yale University Press, New Haven, 1992.
55 R. Brooks, R. E. Bruccoleri, B. D. Olafson, D. J. States, S. Swaminathan and M. Karplus, *J. Comput. Chem.*, 1983, **4**, 187–217.
56 R. A. Laskowski, J. A. Rullmannn, M. W. MacArthur, R. Kaptein and J. M. Thornton, *J. Biomol. NMR*, 1996, **8**, 477–486.
57 J. P. Laussac and B. Sarkar, *Biochemistry*, 1984, **23**, 2832–2838.
58 L. Longenberger and G. Mills, *J. Phys. Chem.*, 1995, **99**, 475–480.
59 J. P. Laussac, M. Pasdeloup and N. Hadjiliadis, *J. Inorg. Biochem.*, 1987, **30**, 227–238.


 